Silicon (2017) 9:543–553
DOI 10.1007/s12633-015-9298-3

ORIGINAL PAPER

Microstructure and *in vitro* Bioactivity of Silicon-Substituted Hydroxyapatite

Huaguang Yu[1,2] · Kejun Liu[1] · Fengmin Zhang[3] · Wenxian Wei[3] · Chong Chen[3] · Qingli Huang[3]

Received: 12 October 2014 / Accepted: 11 May 2015 / Published online: 11 June 2015

Abstract Silicon-substituted hydroxyapatite has shown superior biological performance compared to its stoichiometric counterpart both *in vitro* and *in vivo*. In the present study, single-phase silicon-substituted hydroxyapatite was successfully synthesized by the precipitation method. Chemical composition, crystalline phase, microstructure, and morphology of the materials were characterized by XRF, XRD, FT-IR, solid-state NMR and SEM. The results showed that hydroxyapatite kept its original structure with silicon up to a level of 0.9 wt%. The precipitation method was proved to be an efficient way to synthesize single-phase silicon-substituted hydroxyapatite. Solid-state NMR combined with other techniques gave direct evidence for the isomorphous substitution of PO_4^{3-} by SiO_4^{4-} in the hydroxyapatite structure. Silicon-substituted hydroxyapatite showed better bioactivity than stoichiometric hydroxyapatite in the *in vitro* bioactivity experiment. The higher the silicon content in the hydroxyapatite structure, the better the *in vitro* bioactivity. The enhanced bioactivity of silicon-substituted hydroxyapatite over pure hydroxyapatite has been attributed to the effect of silicate ions in accelerating dissolution.

Keywords Hydroxyapatite · Silicon · Microstructure · *in vitro* bioactivity · Solid-state NMR · SEM

✉ Huaguang Yu
hgyu@yzu.edu.cn

[1] College of Physics Science and Technology, Yangzhou University, Yangzhou 225002, People's Republic of China

[2] Key Laboratory of Mineralogy and Metallogeny, Guangzhou Institute of Geochemistry, Chinese Academy of Sciences, Guangzhou 510460, People's Republic of China

[3] Testing Center, Yangzhou University, Yangzhou 225009, People's Republic of China

1 Introduction

Major components of hard tissues (bones, teeth and some invertebrate skeletons) are composed of hydroxyapatite (HAp) containing various kinds of inorganic substances (such as Na, Mg, Zn, K, Sr, F, Cl, and Si) that occur at trace (1 wt%) levels [1]. Synthetic HAp has been extensively utilized as porous HAp ceramic implants, coating layer on metallic implants, and inorganic filler in HAp–polymer composition materials in orthopedic surgery due to its similar structure to that of the biological apatite [2]. HAp has excellent biocompatibility with hard and soft tissues [3]. The dissolution rate in the body environment is considered as a key indicator since HAp needs to be biologically resorbed by the body in a certain period after implantation. But stoichiometric HAp does not degrade significantly *in vivo* and remains as a permanent fixture for a long time [4]. The stoichiometric HAp does not have sufficient capacity to form an interface with existing bone and to promote the formation of new bone [5].

One way to enhance the bioactivity of HAp is to synthesize substituted apatites, which resemble the chemical composition and structure of the mineral phase in natural bones. Synthesis of chemically modified or ion-substituted HAp has drawn great interest [6, 7]. From the bioactivity point of view, silicon-containing hydroxyapatite could be the most interesting [4]. The concept of addition of silicon to apatite originated from the importance of silicon on bone

formation and calcification and the influence of this element on the bioactivities of bioactive glasses and glass–ceramics [3]. Gibson and his coworkers first reported the synthesis of silicon-containing HAp [8]. Some research indicated that addition of Si to HAp led to superior biological performance compared to stoichiometric counterparts [9–16]. A small amount of Si at a level of 0.5 or 1 wt% was enough to yield obvious bioactivity improvements [4, 17]. The effect of silicon on the bioactivity of HAp has been critically questioned by Bohner [18], due to a lack of deep understanding of the structure of silicon-containing HAp and the origin of the high bioactivity.

It is not clearly understood whether the silicon atoms partially substitute phosphorus atoms in the HAp structure or whether the silicon species remain as independent phases. In some literature, the final products were reported to contain silicon, but their chemical nature was not revealed [19, 20]. The location of Si is crucial to determining the real effects of Si on biological activity. The term silicon-substituted hydroxyapatite (Si-HAp) used herein means that silicon is substituted into the apatite crystal lattice and is not simply added [4].

The bibliography reveals that the amount of silicon that can be incorporated into the structure of HAp without the formation of other species seems to be limited, and the values range from 0.1 to 5 wt% depending on the synthesis methods [4]. Techniques based on FT-IR, Raman, X-ray powder diffraction (XRD), electron spin resonance (ESR) and neutron diffraction do not directly reveal the substitution of P by Si in the HAp structure, especially when Si content is very low [21–23]. X-ray photoelectron spectroscopy (XPS) has been used to investigate the possible replacement of PO_4^{3-} by isolated SiO_4^{4-} in silicon-containing apatites [10, 24]. However, there are many controversial results for the microstructure of Si-HAp reported in publications. Further researches are therefore needed to identify the physical and chemical characteristics of Si-HAp and the correct mechanisms for the positive influence of Si substitution on the bioactivity.

The solid-state nuclear magnetic resonance (NMR) technique was widely used for studying natural bone and synthetic calcium phosphates [25]. Gasquères et al. demonstrated that the exact locations of the silicate entities inside or outside the HAp structure can be determined by solid-state NMR spectroscopy [26]. They observed that in the HAp sample containing 4.6 wt% Si only a fraction of the silicon atoms was incorporated into the HAp lattice in the form of Q^0 (SiO_4^{4-}). Gillespie et al. synthesized ^{29}Si isotopically enriched single phase Si-HAp [27]. Solid-state NMR experiments observed a single peak at −78.2 ppm, and the authors assigned the peak to the Q^1 structure. Hayakawa and coworkers studied the heterogeneous structures of nanocrystalline HAp and Si-HAp synthesized by a wet-chemical procedure by using XRD, TEM, FT-IR and solid-state NMR [28]. They found that a thin amorphous hydrated calcium phosphate layer including hydrated calcium silicate and calcium carbonate covered the crystalline Si-HAp core. Marchat et al. prepared pure Si-HAp using a new precipitation route, and they gave a true precipitation reaction for Si-HAp [29]. They found that $H_3SiO_4^-$ or more basic forms of silicate ions had to be maintained during synthesis to obtain a thermally stable Si-HAp and the silicon content was up to 1.0 wt% in Si-HAp with no secondary phase.

In this study, we try to synthesize stoichiometric HAp and single-phase Si-HAp using precipitation and hydrothermal methods. The object of the current study is to characterize and compare the chemical composition, crystalline phase, microstructure and morphology of different hydroxyapatites, and to obtain a direct and comprehensive understanding of the influences of these factors on physicochemical properties and *in vitro* bioactivities of the materials.

2 Material and Methods

2.1 Sample Preparation

Stoichiometric HAp ($Ca_{10}(PO_4)_6(OH)_2$) and Si-containing HAp were prepared by an aqueous precipitation reaction based on a method described elsewhere [8]. $Ca(NO_3)_2 \cdot H_2O$, $(NH_4)_2HPO_4$ and tetraethyl orthosilicate (TEOS) were used as the starting reactants; see Table 1 for quantities used. The amounts of reagents used were based on the chemical formula $Ca_{10}(PO_4)_{6-X}(SiO_4)_X(OH)_{2-X}$ proposed by Gibson and coworkers [8]. To avoid formation of carbonated apatites, CO_2 dissolved in deionized water was eliminated by boiling the water for 30 min. The volumes of the calcium and phosphate aqueous solutions were fixed at 1000 and 500 ml, respectively. The precipitation reaction was carried out at 90 °C and the pH value of

Table 1 Quantities of reactants used and the expected wt% of silicon

Samples	No. of mole[a]			Si (wt%)
	$Ca(NO_3)_2 \cdot H_2O$	$(NH_4)_2HPO_4$	TEOS	
HAp	1	0.6	0	–
P: $Si\text{-}HAp_{0.8}$	1	0.572	0.028	0.8
P: $Si\text{-}HAp_{1.6}$	1	0.543	0.057	1.6

[a]Ca/P or Ca/(P+Si) is 1.67 for starting materials, uncertainty: 1 %

the solution was maintained at 10.0 by adding ammonia solution (25 %). The reaction mixture was continuously stirred and refluxed until the pH value remained constant (about 168 h). Stoichiometric and Si-containing HAp were prepared by the hydrothermal method [30] using the same reagents. The mixed solution was stirred at 90 °C for 2 h, and subsequently transferred to a hermetically closed Teflon container. The solution was sealed into eight bombs equipped with Teflon liners and then heated at 180 °C for 96 h.

The resulting precipitates were centrifuged and washed several times with deionized water, and then dried at 100 °C overnight. Finally, the powders were placed in alumina crucibles and calcined in a muffle furnace at 950 °C for 24 h in air using a ramp rate of 2.5 °C min^{-1}. P: HAp, P: Si-$HAp_{0.8}$, P: Si-$HAp_{1.6}$, and H: HAp, H: Si-$HAp_{0.8}$, H: Si-$HAp_{1.6}$, represent stoichiometric HAp, Si-HAp with expected Si content (in wt%) of 0.8 wt% and 1.6 wt% synthesized by the precipitation and hydrothermal methods, respectively.

Prior to *in vitro* bioactivity experiments, 500 mg of sieved powders were pressed as disks (13 mm in diameter and 3 mm in height) by uniaxial pressure at 50 MPa and isostatic pressure at 140 MPa. The samples were subsequently placed in alumina crucibles and calcined in air in a muffle furnace at 500 °C for 24 h using heating and cooling rates of 2.5 °C min^{-1}.

2.2 Characterization Techniques

The calcium, phosphorus, and silicon contents of stoichiometric HAp and Si-HAp were determined by a Shimadzu LAB CENTER XRF-1800 sequential X-ray fluorescence spectrometer (XRF). For this analysis, powder samples were shaped into disks (30 mm in diameter) by using a uniaxial pressure of 30 MPa using stainless steel holders. The accuracy of the measurements was verified by use of internal references.

XRD experiments were conducted on a Shimadzu MAXima_X XRD-7000 X-ray powder diffractometer equipped with a Cu anticathode ($\lambda = 1.5406$ Å) and a Ni monochromator, with the X-ray generator operating at 40 kV and 30 mA. The data were collected in the range of $20 - 60°$ with a step size of 0.02° and a count rate of 2.0° min^{-1}. Phase identification was achieved by comparing the diffraction patterns of HAp and Si-HAp with International Center for Diffraction Data (ICDD) standard PDF cards. The structural parameters of HAp and Si-HAp were obtained by Rietveld refinement of the XRD data, and the refinements were based on the structural data of Kay et al. using the space group $P6_3/m$ [31]. FT-IR spectra were recorded using a Varian Cary 610 FT-IR spectrometer. The samples were embedded in KBr pellets at room temperature, and the spectra were recorded at 4 cm^{-1} resolution averaging 96 scans.

All the solid-state NMR experiments were carried out at B_0 = 9.4 T on a Bruker AVANCE III 400 WB NMR spectrometer. The corresponding resonance frequencies of ^{1}H, ^{31}P and ^{29}Si were 400.15, 161.98 and 79.49 MHz, respectively. ^{1}H and ^{31}P magic angle spinning (MAS) NMR spectra were acquired with a 4 mm HX probehead, and the MAS frequency was 15 kHz. ^{1}H MAS NMR spectra were acquired using a rotor-synchronized Hahn echo pulse sequence to minimize the background. The $\pi/2$ pulse length was 2.4 μs, and the echo delay was 67 μs. 80 transients were accumulated with a recycle delay of 20 s. ^{31}P MAS NMR spectra were acquired using direct excitation with ^{1}H high power decoupling. $\pi/2$ pulse length was 3.0 μs, and 32 transients were accumulated with a recycle delay of 120 s. For ^{29}Si direct excitation with ^{1}H high power decoupling experiments, the samples were packed in a 7 mm ZrO_2 rotor, and the MAS frequency was 5 kHz. The spectrum was acquired using a $\pi/2$ pulse length of 6.0 μs and a recycle delay of 60 s. The long recycle delays were used for all the MAS NMR experiments to allow complete relaxation of the resonances to be able to compare the relative intensities of the peaks, especially for the ^{29}Si MAS NMR spectra. For ^{1}H $\rightarrow$ ^{29}Si cross polarization magic angle spinning (CP/MAS) NMR experiments, the Hartmann–Hahn condition was carefully optimized using kaolinite in order to enhance the magnetization transfer between the ^{1}H and ^{29}Si reservoirs. Two contact times, 1.0 and 4.6 ms, were used in the experiments. Both ^{1}H and ^{29}Si chemical shifts were externally referenced to TMS, while the ^{31}P chemical shift was referenced to 85 % H_3PO_4 solution.

For $T_{1\rho}$ (^{1}H) filter ^{1}H $\rightarrow$ ^{29}Si CP/MAS NMR experiments, the pulse sequence (Fig. 1) is primarily based on differences in $T_{1\rho}$ (^{1}H), the characteristic time of the

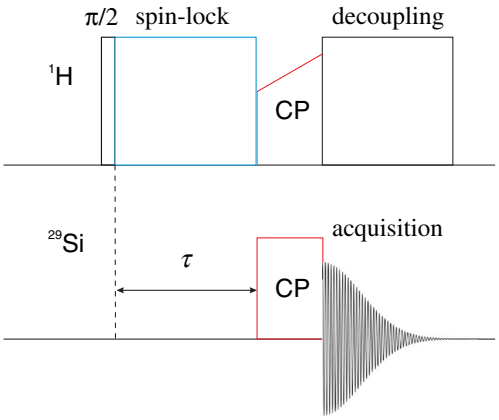

Fig. 1 The pulse sequence for $T_{1\rho}$ (^{1}H) filter ^{1}H $\rightarrow$ ^{29} Si CP/MAS NMR

spin–lattice relaxation in the rotating frame. Before the CP transfer, a ^{1}H spin-lock evolution during τ is added, which can be set so as to nullify the magnetization of one signal with short $T_{1\rho}$ (^{1}H), resulting in only the signal of the other with longer $T_{1\rho}$ (^{1}H) being observed. $T_{1\rho}$ (^{1}H) values for the structural OH^- groups of HAp and for adsorbed H_2O are 12 and 0.6 ms [26], respectively. For τ = 10 ms, CP occurs mainly from the structural OH^- groups.

The microstructures of the materials were investigated on a Hitachi S-4800 field emission scanning electron microscope (SEM) operating at 10 kV.

2.3 *In vitro* Bioactivity Tests

In vitro bioactivities of the samples were verified by the method previously described, and the simulated body fluid (SBF) was prepared using the standard protocol of Kokubo [32]. Although the use of the SBF method for bioactivity tests has been questioned by some authors, particularly Bohner and Lemaitre [33], and Pan and coworkers [34], it has been widely used for *in vitro* bioactivity tests for many biomaterials. All of the experiments were carried out in plastic containers not containing silicon rather than a glass container to avoid the interference from silicon released from the glass. The sintered apatite disks were soaked in 400 ml of SBF with ionic concentrations nearly equal to those of human serum, a pH value of 7.4, and a temperature of 37 °C. Disks were placed in specially designed galvanized iron wire scaffolds and hung with a thin line, which allowed the entire material to be exposed to the fluid. The samples were taken out of the fluid after 1, 3, 5, 7, 10, 14, 20 and 25 days of soaking, then gently washed with distilled water, and dried at 100 °C for 2 hours. The dried samples were used for further characterization, such as XRD, FT-IR and SEM analysis, to reveal the formation of apatite layers on the surface of the samples. At each time point, Ca, P and Si ion concentrations of SBF solutions were measured by a PerkinElmer Optima 7300 V inductively coupled plasma atomic emission spectrometer (ICP-AES). The rate of new apatite formation was considered as a measure of bioactivity of the material.

3 Results and Discussion

3.1 XRF Analysis

The expected values and XRF results of the samples are listed in Table 2 for comparison. The experimental silicon content values indicate that the synthesized samples do not contain the whole silicon quantities from TEOS. It is obvious that silicon was not incorporated into HAp for the samples prepared by the hydrothermal method. The presence of low amounts of Si in the H: HAp and P: HAp samples may be from the starting reactants used in the preparation or from the glass containers. Although plastic containers were used; according to Kokubo and Takadama' s advice for *in vitro* bioactivity tests [32], we can not exclude the presence of small amounts of Si in reactants used for the synthesis and the release of Si from glass containers in the preparation processes. Marchat et al. found that soluble silicates prepared from TEOS *via* a sol-gel route, $H_3SiO_4^-$ or more basic forms of silicate ions, had to be maintained during synthesis to obtain a thermally stable Si-HAp without other phases, and keeping the pH value at 10.8 was important to obtain HPO_4^{2-} and $H_3SiO_4^-$ ions in solution as the main phosphate and silicates, respectively [29]. In the hydrothermal condition, we can control the pH value of the mixed solution before it was transferred to the hermetically closed Teflon containers, but we can not adjust the pH value in the closed containers. With the progress of reaction in the closed containers, the pH value will decrease, and that may be the reason that little silicon was incorporated in HAp in the hydrothermal method. From Table 2, both the Ca/P and Ca/(P+Si) molar ratios of the materials were higher than the expected values, while the Ca/(P+Si) molar ratios remained almost constant. These results show the samples had small deviation from stoichiometry.

Table 2 Expected and XRF experimental molar ratios and wt% of silicon

Samples	Ca/P ratio		Ca/(P+Si) ratio		Si (wt%)	
	Expected	Experimental	Expected	Experimental	Expected	Experimental
P: HAp	1.67	1.70	1.67	1.69	–	0.2 ± 0.1
P: Si-HAp$_{0.8}$	1.75	1.73	1.67	1.69	0.8	0.6 ± 0.1
P: Si-HAp$_{1.6}$	1.84	1.79	1.67	1.69	1.6	0.9 ± 0.1
H: HAp	1.67	1.71	1.67	1.68	–	0.2 ± 0.1
H: Si-HAp$_{0.8}$	1.75	1.71	1.67	1.70	0.8	0.2 ± 0.1
H: Si-HAp$_{1.6}$	1.84	1.71	1.67	1.69	1.6	0.2 ± 0.1

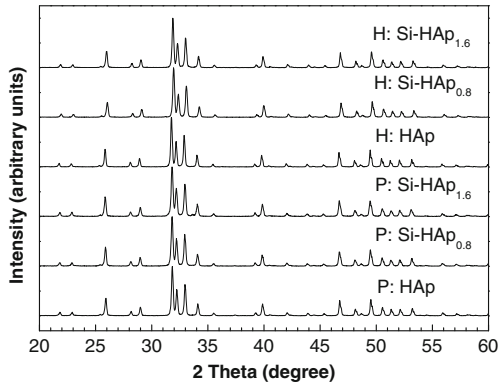

Fig. 2 XRD patterns of HAp and Si-HAp

3.2 XRD Analysis

The XRD patterns for the samples are shown in Fig. 2. All the diffraction peaks matched the ICDD standards for HAp (JCPDS-ICDD-PDF#-09-0432). No other phases, such as α- or β-tricalcium phosphate (TCP), calcium silicate and calcium carbonate, were observed. The absence of broad peaks suggested no amorphous phases existed. Gibson et al. [35] investigated the effect of silicon substitution on the sintering and microstructure of HAp. They found that silicon is incorporated at a level of up to 1.6 wt%, and that the phase composition remained the same as for HAp, with no secondary phases being formed using a low sintering temperature (1000 − 1150 °C) [35]. It has been shown by Kim et al. [36] that if Si substitution was above 2 wt%, α-TCP was formed. Recently, Qiu et al. [37] demonstrated that there is only pure HAp phase in the 0.8 wt% Si-doped HAp sample, while a small quantity of α-TCP existed in the 1.6 wt% Si-doped HAp sample and α-TCP, β-TCP, and silicocarnotite ($Ca_5(PO_4)_2SiO_4$) phases were detected in the 2.0 wt% Si-doped HAp sample. For the XRD results of samples with Si content of 4 wt% and above, only β-TCP remained, and the HAp phase disappeared [37]. In the present study, the amounts of Si were relatively low, and the sintering temperature was 950 °C. But when TEOS was added corresponding to a Si level of 2.4 wt% and above, secondary phases were detected (data not shown). Some authors [28] found that HAp with the silicon content up to 4.6 wt% kept its structure, but heterogeneous structure was found by solid-state ^{31}P NMR experiments. The amount of incorporated silicon has an important influence on thermal stability. After heating at 950 °C, samples with Si content up to 0.9 wt% remained as a single apatite phase, whereas higher Si content led to decomposition of HAp. Our results agree with those of Marchat [29], and the highest Si content in their synthesis of single phase Si-HAp was 1.0 wt%.

Several methods for synthesis of Si-HAp have been reported [29, 30, 35, 37–39]; the controlled crystallization method is, by far, the most common synthesis route [8, 40]. In the present study, the hydrothermal method failed to synthesize single-phase Si-HAp. We tried several times with varying conditions, but none were successful. Either there were secondary phases or Si was not incorporated into the HAp lattice. However, the precipitation method was a simple route for the preparation of Si-HAp. This method is similar to the controlled crystallization method, and the reaction time needed is very long considering that HAp is thermodynamically the most stable among all calcium phosphates [25].

H: HAp, H: Si-HAp_X and P: HAp samples exhibited higher intensity and narrower diffraction peaks in XRD patterns compared to those of P: Si-$HAp_{0.8}$ and P: Si-$HAp_{1.6}$ samples, indicating larger crystallite size and higher crystallinity. For samples prepared by the precipitation method, the reflections became wider and less intense as the Si content increased. This may be a consequence of the loss of crystallinity due to the formation of hydroxyl vacancies caused by the isomorphous substitution of PO_4^{3-} by SiO_4^{4-}, or it may be due to the effect of smaller crystallite size [35, 41].

The effect of Si incorporation on HAp structure parameters was determined by Rietveld structure refinement of the XRD data. The lattice parameters and the unit cell volume are shown in Table 3. The radius of Si^{4+} (0.42 Å) is greater than that of P^{5+} (0.35 Å), and the length of the Si–O bond (0.161 nm) is greater than that of the P–O bond (0.155 nm)

Table 3 Lattice parameters for stoichiometric HAp and Si-HAp

Samples	*a* axis (Å)	*c* axis (Å)	Volume (Å^3)
P: HAp	9.41081	6.88059	527.73
P: Si-$HAp_{0.8}$	9.41586	6.88570	528.69
P: Si-$HAp_{1.6}$	9.41409	6.89377	529.11
H: HAp	9.42430	6.88566	529.63
H: Si-$HAp_{0.8}$	9.39222	6.86267	524.28
H: Si-$HAp_{1.6}$	9.40399	6.87068	526.21

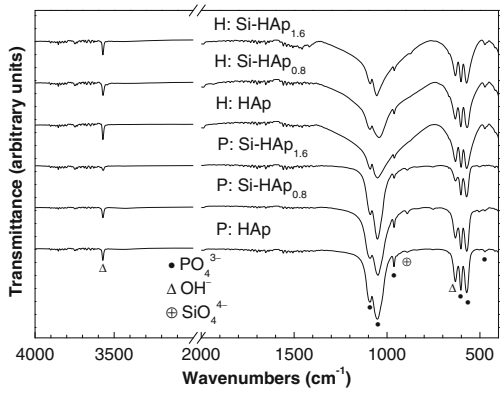

Fig. 3 FT-IR spectra of HAp and Si-HAp

[4]. The radius of the SiO_4^{4-} is expected to be greater than that for the PO_4^{3-}, which may result in the change of HAp lattice constants. There is no obvious relationship between lattice parameters and Si incorporation in the present study. The crystal lattice variations of Si-HAp with the increases of Si content from previous studies [8, 12, 30, 38, 42, 43] are quite different, and even opposite results were obtained. Recently, Qiu et al. [37] obtained the slow-scanning XRD data of the as-prepared pure HAp and Si-HAp with Si doping percentage from 0.4 to 1.6 wt%. Their refined results show that with the increase of Si content, the length of the *a* axis keeps increasing, while the length of the *c* axis firstly increases and then becomes stable. The cell volume always increases and the density accordingly decreases with the increasing Si doping percentage [37].

3.3 FT-IR Analysis

In the FT-IR spectra of the materials (Fig. 3), the stretching and vibration modes of the OH^- groups were observed at about 3571 cm^{-1} (ν_S) and 632 cm^{-1} (ν_L), and the vibration mode of the PO_4^{3-} groups: ν_1 at 961 cm^{-1}, ν_2 at 473 cm^{-1}, ν_3 at 1041 cm^{-1} and 1090 cm^{-1}, and ν_4 at 602 and 571 cm^{-1}, respectively. There were no vibration bands at 1456 and 1413 cm^{-1}, suggesting that A-site and B-site CO_3^{2-} substitution had not occurred. It has been suggested that boiling of water for 30 min is a promising method for eliminating CO_2 dissolved in water, by restricting the absorption of CO_2 in air during preparation. Since SiO_4^{4-} and CO_3^{2-} are known to competitively replace PO_4^{3-} sites [6, 8], restricting the presence of CO_3^{2-} should favor the incorporation of the former. An additional weak band appearing at 891 cm^{-1} for the samples prepared by the precipitation method is related to the presence of the SiO_4^{4-} group in the apatite structure [29, 44]; the intensity of this band increased with increasing amounts of Si. It is reported that the bending vibration of Si–O–Si for the polymerization of SiO_4^{4-} will produce a band at 800 cm^{-1} in the FT-IR spectrum [45]. In the present work, no bands appear at 800 cm^{-1}.

Band intensities corresponding to PO_4^{3-} (most noticeably at about 961 cm^{-1}) and OH^- (3571 and 632 cm^{-1}) groups of the samples prepared by the precipitation method distinctly decreased as Si content increased, which verify the loss of hydroxyl groups in Si-HAp. This behavior is associated with the substitution of SiO_4^{4-} for some PO_4^{3-} sites, which reduced the amounts of OH^- groups to balance the charge [46], leading to the creation of hydroxide vacancies [43]:

$$Ca_{10}(PO_4)_{6-X}(SiO_4)_X(OH)_{2-X}\square_X \quad (0 \leqslant X \leqslant 2) \qquad (1)$$

wherein, □ represents the vacancy at the position of the hydroxyl group.

3.4 Solid-state NMR

Pure HAp is in the hexagonal space group $P6_3/m$ [31, 47]. All the P atoms are crystallographically equivalent, and the structural hydroxyl groups of HAp are crystallographically equivalent and located at the edges of unit cells in the –O-H O-H O-H O-H– columns, while there are two calcium sites in the crystal structure [31, 47]. Each P atom has two proton neighbours at 3.847 Å and a further two at 4.205 Å, while the others are 6 Å or more away. The homonuclear (^{31}P–^{31}P and ^{1}H–^{1}H) and heternuclear (^{1}H –^{31} P) dipolar couplings in HAp can easily be overcome by MAS at several kilohertz [25].

Proton MAS NMR spectra are shown in Fig. 4a. The major peak at 0.2 ppm is attributed to the structural hydroxyl group [25]. The minor peak at ca. 1.6 ppm has been extensively reported in the solid-state NMR analysis of HAp, and the source of this signal is controversial [48, 49]. Broad peaks appear at ca. 5.4 ppm in P: Si-$HAp_{0.8}$ and P: Si-$HAp_{1.6}$ samples. Hartmann et al. stated that these peaks arise from OH^- groups which are adjacent to vacancies in the OH^- substructure by using two-dimensional double-quantum correlation NMR [48]. Some authors assigned the peak at ca. 5.4 ppm to water molecules adsorbed on the surface of HAp [28, 50, 51]. All the direct excitation ^{31}P MAS NMR spectra (Fig. 4b) invariably have a predominant peak at ca. 2.8 ppm, which is assigned to the PO_4^{3-} group [25]. Extra ^{31}P NMR peaks with weak intensities at ca. 5.8 ppm in P: Si-$HAp_{0.8}$ and P: Si-$HAp_{1.6}$ may be assigned to PO_4^{3-} groups that lack a nearby OH^- group [48, 49]. For the samples prepared by the precipitation method, the full widths at half-maximum (FWHM) of the peaks at 0.2 ppm in the ^{1}H MAS NMR spectra and the peaks at 2.8 ppm in the ^{31}P MAS NMR spectra increase with Si content. The broadening of these peaks suggests an increase in the local disorder about these samples where silicon has been incorporated into the HAp structure.

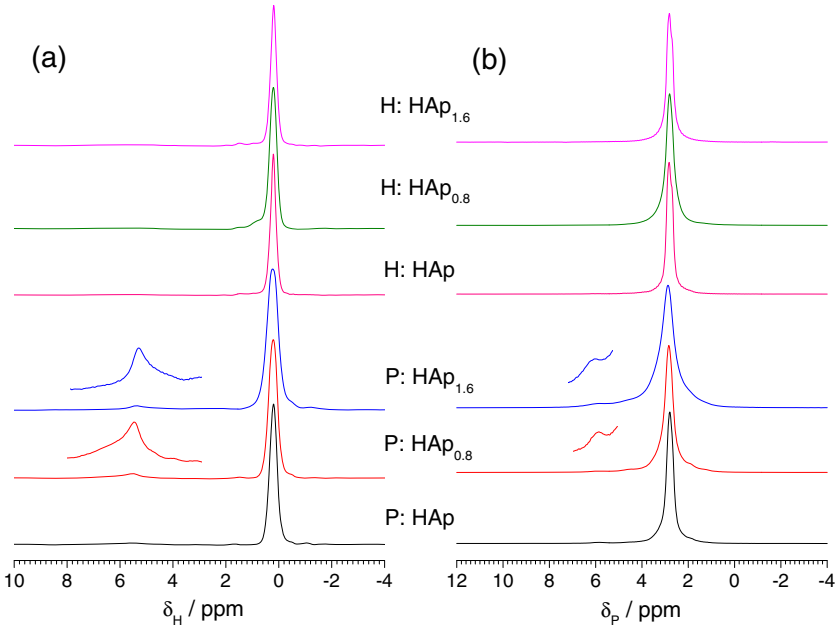

Fig. 4 Solid-state ^{1}H (**a**) and ^{31}P (**b**) MAS NMR spectra of HAp and Si-HAp

Direct excitation ^{29}Si MAS NMR spectra of P: Si-HAp$_{1.6}$ are depicted in Fig. 5a. Two resonances at −72.8 and −69.4 ppm, corresponding to Q^0 units, were observed. No resonances corresponding to Q^2, Q^3 and Q^4 (expected between −85 and −110 ppm) were identified within the detection limits of the solid-state NMR techniques used here. Gasquères [26] and Marchat [29] also observed the sharp resonance located at ca. −72.8 ppm, and they assigned it to SiO_4^{4-} inside the HAp structure. In ^{1}H →^{29}Si CP/MAS NMR experiments with contact times of 1.0 and 4.6 ms (Fig. 5b and c), the resonance at −72.8 ppm is still observed, but the relative intensities of the signal at −69.4 ppm were significantly reduced. Gomes et al. assigned the resonance at −69 ppm to silicate sites in β-TCP [52]. They assumed that the peak at −73 ppm also contains a contribution from silicate ions in β-TCP [52]. But this assignment is questionable. If the peak at −69 ppm and partial contribution of the peak at −73 ppm are assigned to β-TCP, this component should be detected by XRD due to its large proportion for their sample. Thus, the resonance at −69.4 ppm is tentatively assigned to SiO_4^{4-} groups that lack adjacent OH^- groups. This phenomenon indicates the absence of protons within 3.847 Å or an even longer distance to the corresponding silicon atoms (the shortest proton-phosphorus distance is 3.847 Å in HAp [31, 47]). However, when the amount of TEOS added corresponded to a Si level of 2.4 wt% and above, a broad peak (ca. −110 ppm) corresponding to polymeric silicate species (Q^3/Q^4) was detected (data not shown). This result suggests that for samples richer in Si, a substantial fraction of the Si atoms present in the solid belong to extra framework silicate species. In the $T_{1\rho}$ (^{1}H) filter ^{1}H → ^{29}Si CP/MAS NMR experiments (Fig. 5d and e), the ^{1}H spin-lock evolution during τ was set to 10 ms (the $T_{1\rho}$ (^{1}H) values for the O^{1}H of HAp and $^{1}H_2O$ were 12 and 0.6 ms [26], respectively) to ensure that magnetization transfer originated only from the structural O^{1}H groups of HAp. The peak at −72.8 ppm was still obvious. The detected ^{29}Si resonances therefore correspond to Si nuclei dipolar coupled to O^{1}H protons and located inside the HAp structure [26]. The absence of resonance at −69.4 ppm in the ^{1}H → ^{29}Si CP/MAS NMR spectra is attributed to lack of adjacent OH^- groups due to loss of these groups at some sites. Hence, the solid-state NMR experiments

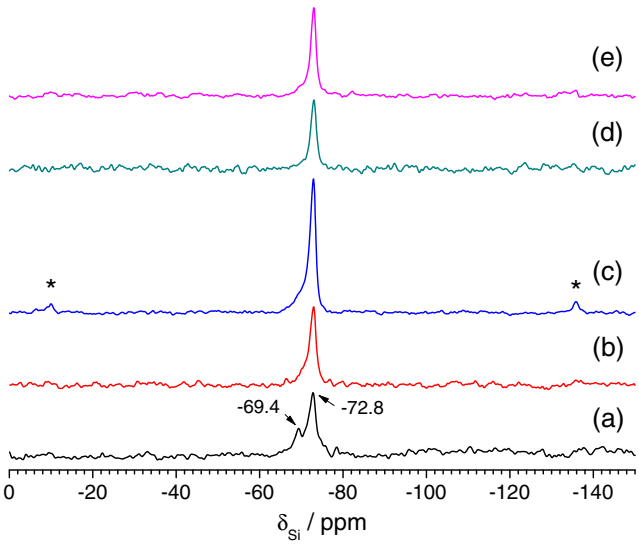

Fig. 5 Solid-state ^{29}Si MAS NMR spectra of P: Si-HAp$_{1.6}$ acquired with direct excitation (**a**); and with ^{1}H→ ^{29}Si CP/MAS with contact times of 1.0 ms (**b**) and of 4.6 ms (**c**); and with $T_{1\rho}$ (^{1}H) filter ^{1}H→ ^{29}Si CP/MAS with contact times of 1.0 ms (**d**) and of 4.6 ms (**e**). The star sign (*) denotes spinning sideband

clearly demonstrate that silicon atoms belonging to isolated SiO_4^{4-} anions isomorphically substituted PO_4^{3-} anions in the apatite structure. ^{29}Si NMR signals were not detected for other samples due to the low amount of ^{29}Si in the samples (high detection limit).

3.5 SEM

Representative SEM micrographs of the samples are illustrated in Fig. 6. Samples synthesized *via* the precipitation method are round particles and plate-like crystals, while those prepared by the hydrothermal process are plate-like and nonuniform in size. The grain sizes of the samples prepared by the precipitation method are clearly finer than those samples prepared by the hydrothermal method. There have been some reports on the effect of Si on the grain size of Si-HAp. Palard et al. [20] and Li et al. [53] reported that the grain size of Si-HAp decreased with increasing Si content, and that the grain size decreased less when the Si content reached a certain value due to the formation of secondary phases such as α-TCP. Gibson and coworkers [35] suggested that a higher value of activation energy (183 −205 kJ mol^{-1}) was required for the growth of the grains for Si-HAp compared to those for stoichiometric HAp (141 kJ mol^{-1}). This indicates that Si effectively impedes the grains from coarsening during heat treatment. In the present study, there was no obvious difference in the grain sizes for the samples prepared by the precipitation method.

3.6 *In vitro* Tests

Plots of Ca, P and Si ion concentrations in SBF solution as a function of time after immersion of the samples are shown in Fig. 7. These results helped to explore the changes in the *in vitro* behavior of the samples with respect to Si substitution. The ion concentration variations at different periods indicated that ion exchange took place between the samples and the SBF solutions.

Ca ion concentration decreased very rapidly at the beginning, and reached a quasi-stationary state after 10 days. Pronounced decreases in Ca ion concentration of the SBF solution were observed after only 1 day for P: Si-$HAp_{0.8}$ and P: Si-$HAp_{1.6}$. Ca consumption and Si release by the samples prepared by the precipitation method increased with the increasing Si content. The samples prepared by the hydrothermal method showed lower activity in trapping Ca from the SBF solution. The decrease of P concentration as a function of time was almost identical for all the

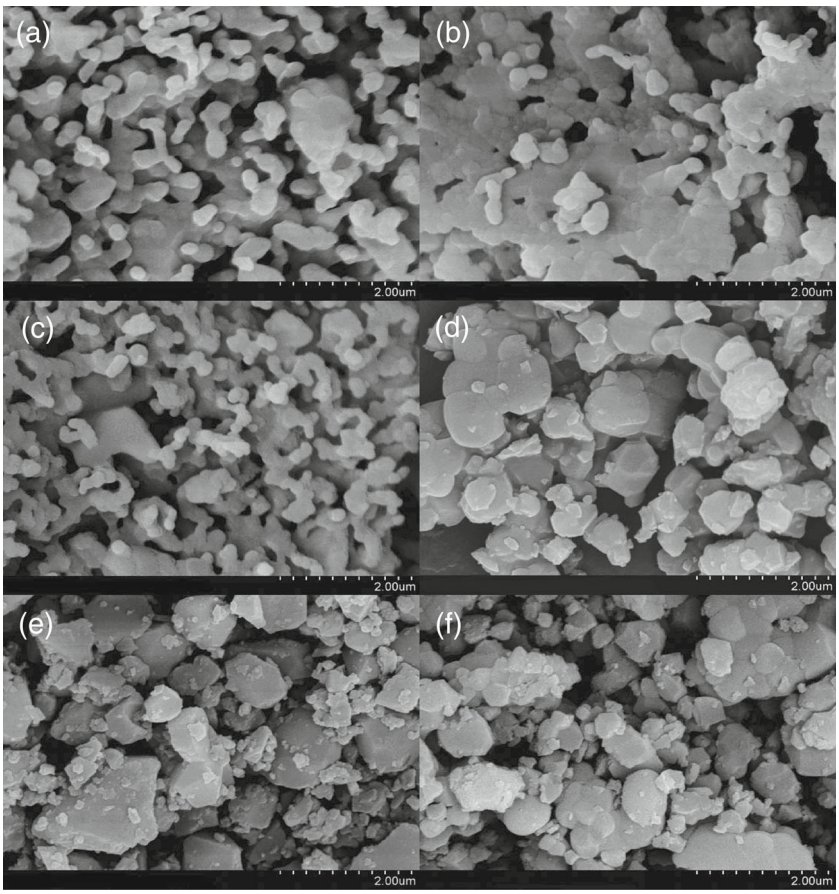

Fig. 6 SEM micrographs of HAp and Si-HAp granules **a** P: HAp; **b** P: Si-$HAp_{0.8}$; **c** P: Si-$HAp_{1.6}$; **d** H: HAp; **e** H: Si-$HAp_{0.8}$; and **f** H: Si-$HAp_{1.6}$

samples. Thian et al. observed that the Ca and P ion levels in the SBF remained approximately constant during the initial immersion period, and a significant decline was observed after 14 days of immersion for the as-sputtered and annealed Si-HAp thin coatings samples [54]. Balas and coworkers [10] observed no significant change of P concentration in the first 2 weeks and the increment after 3 weeks for P concentration. They argued that this may be ascribed to dissolution of the surface layer, but Ca concentration decreased very rapidly at the beginning and reached a quasi-stationary state after 3 weeks. The rapid decrease of Ca and P ion concentrations in the SBF solution suggests that new apatite layers formed on the surface of Si-HAp after a short time in SBF solution.

Figure 7 illustrates the rapid release of Si at the beginning from P: Si-HAp$_{0.8}$ and P: Si-HAp$_{1.6}$ samples immersed in SBF solution compared to P: HAp. Dissolution was observed to follow the order P: Si-HAp$_{1.6}$ >P: Si-HAp$_{0.8}$ > P: HAp, suggesting that the silicate increased the solubility.

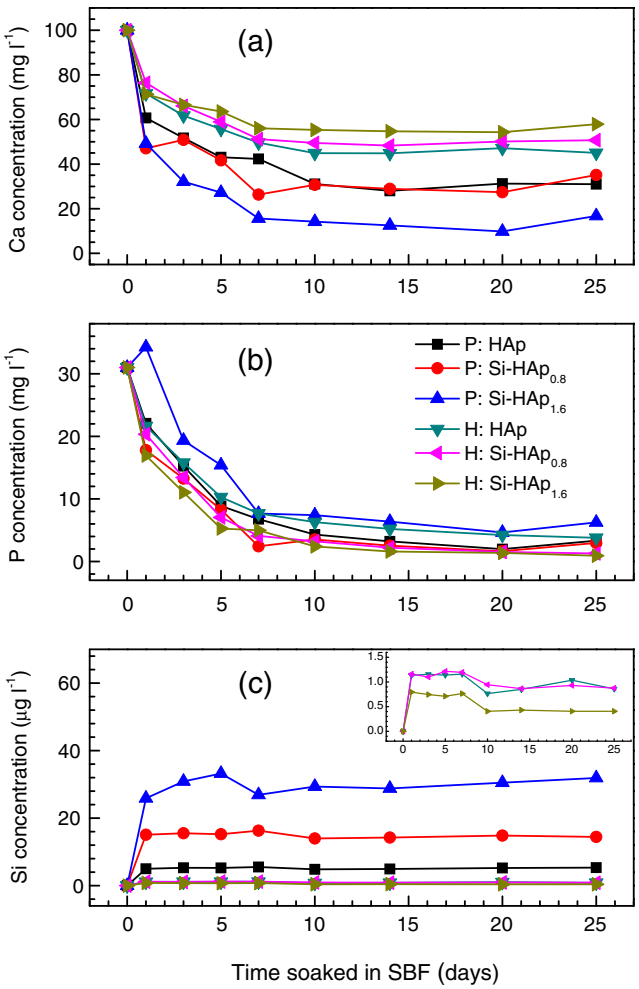

Fig. 7 Calcium, phosphorous and silicon concentrations of SBF solution versus soaking time

For P: Si-HAp$_{1.6}$ with the highest Si content, the Si concentration of SBF after 5 days was up to 34 μg l^{-1} followed by a slight decrease. High-resolution transmission electron microscopy (TEM) was used to observe dissolution of HAp and Si-HAp implants after 6 and 12 weeks *in vivo* and in acellular SBF by Porter and his coworkers [11, 13, 55]. Dissolution was observed to follow the order 1.5 wt% Si-HAp > 0.8 wt% Si-HAp > pure HAp. Dissolution was found to be particularly prevalent at grain boundaries and triple-junctions *in vivo* [11], while it predominated at the crystallite surfaces in SBF [13]. Pietak et al. [1] pointed out that aqueous Si has dose-dependent effects on osteoblast differentiation, proliferation and collagen synthesis, osteoclast formation and the resorption process, as well as implications for the formation of the extracellular matrix and the biomineralization process. The release of Si complexes in the form of Si(OH)$_4$ from the implant may therefore stimulate tissue regeneration and affect the remodeling process [1].

The rapid release of Si and decrease of Ca in the SBF solution in the early period of our *in vitro* tests was in accord with the results of *in vivo* studies carried out by Patel and coworkers [9], which showed that the early bioactivity of hydroxyapatite is significantly improved with the incorporation of silicate ions into the HAp structure. The changes of Ca, P, and Si concentration indicated that dissolution and precipitation occurred simultaneously after immersion of the samples in SBF solution. Porter proposed the dissolution–reprecipitation mechanism of apatite nucleation [55]. The dissolution of calcium and phosphate ions released from the bioceramic surface increases their local concentration leading to the formation of biological apatite.

The formation of surface layers on the materials can be conveniently monitored by SEM. Figure 8 shows SEM micrographs of the materials after 25 days soaked in SBF solution. XRD results confirmed these deposits to be crystalline apatite. Plate-like apatite crystallites appeared to emanate from the surface of the samples prepared by the precipitation method. Si had a positive effect on both dissolution and reprecipitation processes of apatite. Large, flower-like crystallites were observed on the surface of P: Si-HAp$_{1.6}$. In some regions, the formation of new apatite seemed to connect the grains. In comparison, worm-like deposits were observed on the surfaces of the samples prepared by the hydrothermal method. The degree of deposits formation on these samples was similar. P: HAp and the samples prepared by the hydrothermal method possessed the same chemical compositions, but nevertheless they exhibited differences in their capacity to induce the formation of the apatite-like layer.

Although the high bioactivity mechanism for Si-HAp may be difficult to explain, our *in vitro* bioactivity results in SBF solution clearly demonstrate an increase of reactivity when silicon is incorporated. It appears likely that Si

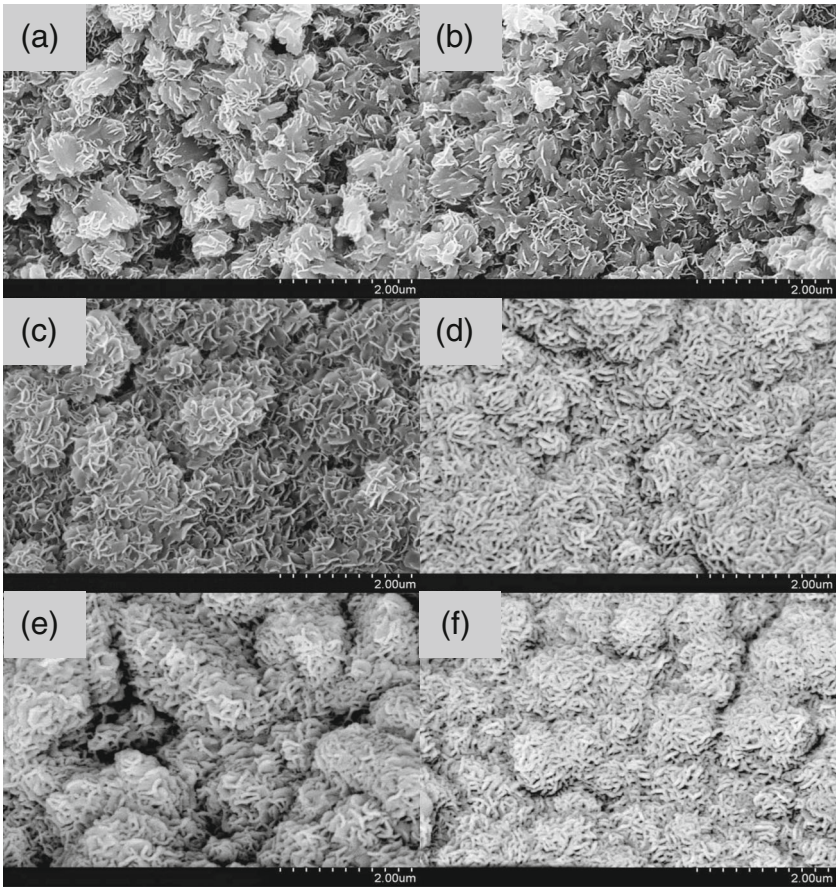

Fig. 8 SEM images of HAp and Si-HAp after 25 days in SBF **a** P: HAp; **b** P: Si-$HAp_{0.8}$; **c** P: Si-$HAp_{1.6}$; **d** H: HAp; **e** H: Si-$HAp_{0.8}$; and **f** H: Si-$HAp_{1.6}$

promotes apatite precipitation on Si-HAp by a combination of increasing the solubility of the materials *via* creation of defects in the lattice [1, 22, 55], and by generating a more electronegative surface [56] and a smaller grain size with more triple-junctions per unit area, facilitating increased dissolution at the surface [55]. We will try to clarify the major role of silicon in the dissolution and reprecipitation processes in our future research.

4 Conclusions

Silicon-substituted hydroxyapatites were prepared by the precipitation method, and their microstructure and *in vitro* bioactivities were examined. The results revealed that the precipitation method is a good procedure for preparation of single-phase silicon-substituted hydroxyapatites that can be used as a potential material for prosthetic applications. The influence of the silicon content on the structure and *in vitro* bioactivity of the resulting materials was studied. The amount of silicon that can be incorporated seems to be limited; 0.9 wt% was the highest Si content in the samples studied. Solid-state NMR clearly demonstrated that Si ions are incorporated within the hydroxyapatite lattice, and do not only cover the surface. We have demonstrated that solid-state NMR is an invaluable tool to investigate the microstructure of silicon-substituted hydroxyapatite. The current findings confirmed that incorporation of Si into apatite led to solubility enhancements of the HAp substrate, and resulted in pronounced bioactivity *in vitro*. The mechanism of silicon leading to improved bioactivity requires further investigation.

Acknowledgments The authors acknowledge the financial support from the Natural Science Foundation of China (No. 21005069) and Key Laboratory of Mineralogy and Metallogeny, Guangzhou Institute of Geochemistry, Chinese Academy of Sciences (KLMM20120202).

References

1. Pietak AM, Reid JW, Stott MJ, Sayer M (2007) Biomaterials 28:4023. doi:10.1016/j.biomaterials.2007.05.003
2. Dorozhkin SV, Epple M (2002) Angew Chem Int Ed 41:3130. doi:10.1002/1521-3773
3. Hench LL, Wilson J (eds) (1993) An Introduction to Bioceramics, vol 1. World Scientific, Florida
4. Vallet-Regí M, Arcos D (2005) J Mater Chem 15:1509. doi:10.1039/b414143a
5. Khan AF, Saleem M, Afzal A, Ali A, Khan A, Khan AR (2014) Mater Sci Eng C 35:245. doi:10.1016/j.msec.2013.11.013
6. Gibson IR, Bonfield W (2002) J Biomed Mater Res 59:697. doi:10.1002/jbm.10044

7. Shepherd JH, Shepherd DV, Best SM (2012) J Mater Sci Mater Med 23:2335. doi:10.1007/s10856-012-4598-2
8. Gibson IR, Best SM, Bonfield W (1999) J Biomed Mater Res 44:422. doi:10.1002/(SICI)1097-4636
9. Patel N, Best SM, Bonfield W, Gibson IR, Hing KA, Damien E, Revell PA (2002) J Mater Sci Mater Med 13:1199. doi:10.1023/a:1021114710076
10. Balas F, Perez-Pariente J, Vallet-Regí M (2003) J Biomed Mater Res 66A:364. doi:10.1002/jbm.a.10579
11. Porter AE, Patel N, Skepper JN, Best SM, Bonfield W (2003) Biomaterials 24:4609. doi:10.1016/s0142-9612(03)00355-7
12. Porter AE, Best SM, Bonfield W (2004) J Biomed Mater Res 68A:133. doi:10.1002/jbm.a.20064
13. Porter AE, Botelho CM, Lopes MA, Santos JD, Best SM, Bonfield W (2004) J Biomed Mater Res 69A:670. doi:10.1002/jbm.a.30035
14. Botelho CM, Brooks RA, Best SM, Lopes MA, Santos JD, Rushton N, Bonfield W (2006) J Biomed Mater Res 79A:723. doi:10.1002/jbm.a.30806
15. Thian ES, Huang J, Best SM, Barber ZH, Bonfield W (2007) Mater Sci Eng C 27:251. doi:10.1016/j.msec.2006.05.016
16. Manzano M, Lozano D, Arcos D, Portal-Nunez S, Lopez la Orden C, Esbrit P, Vallet-Regí M (2011) Acta Biomater 7:3555. doi:10.1016/j.actbio.2011.06.004
17. Hing KA, Revell PA, Smith N, Buckland T (2006) Biomaterials 27:5014. doi:10.1016/j.biomaterials.2006.05.039
18. Bohner M (2009) Biomaterials 30:6403. doi:10.1016/j.biomaterials.2009.08.007
19. Thian ES, Huang J, Best SM, Barber ZH, Bonfield W (2005) Biomaterials 26:2947. doi:10.1016/j.biomaterials.2004.07.058
20. Palard M, Combes J, Champion E, Foucaud S, Rattner A, Bernache-Assollant D (2009) Acta Biomater 5:1223. doi:10.1016/j.actbio.2008.10.016
21. Reid JW, Pietak A, Sayer M, Dunfield D, Smith TJN (2005) Biomaterials 26:2887. doi:10.1016/j.biomaterials.2004.09.005
22. Pietak AM, Reid JW, Sayer M (2005) Biomaterials 26:3819. doi:10.1016/j.biomaterials.2004.10.013
23. Gomes S, Nedelec JM, Jallot E, Sheptyakov D, Renaudin G (2011) Cryst Growth Des 11:4017. doi:10.1021/cg200587s
24. Botelho CM, Lopes MA, Gibson IR, Best SM, Santos JD (2002) J Mater Sci Mater Med 13:1123. doi:10.1023/a:1021177601899
25. Kolodziejski W (2005). In: Klinowski J (ed) New techniques in solid-state NMR, Topics in Current Chemistry, vol 246. Springer, Berlin, pp 235–270. doi:10.1007/b98652
26. Gasquères G, Bonhomme C, Maquet J, Babonneau F, Hayakawa S, Kanaya T, Osaka A (2008) Magn Reson Chem 46:342. doi:10.1002/mrc.2109
27. Gillespie P, Wu G, Sayer M, Stott MJ (2010) J Mater Sci Mater Med 21:99. doi:10.1007/s10856-009-3852-8
28. Hayakawa S, Kanaya T, Tsuru K, Shirosaki Y, Osaka A, Fujii E, Kawabata K, Gasquères G, Bonhomme C, Babonneau F, Jäger C, Kleebe HJ (2013) Acta Biomater 9:4856. doi:10.1016/j.actbio.2012.08.024
29. Marchat D, Zymelka M, Coelho C, Gremillard L, Joly-pottuz L, Babonneau F, Esnouf C, Chevalier J, Bernache-assollant D (2013) Acta Biomater 9:6992. doi:10.1016/j.actbio.2013.03.011
30. Tang XL, Xiao XF, Liu RF (2005) Mater Lett 59:3841. doi:10.1016/j.matlet.2005.06.060
31. Kay MI, Young RA, Posner AS (1964) Nature 204:1050. doi:10.1038/2041050a0
32. Kokubo T, Takadama H (2006) Biomaterials 27:2907. doi:10.1016/j.biomaterials.2006.01.017
33. Bohner M, Lemaitre J (2009) Biomaterials 30:2175. doi:10.1016/j.biomaterials.2009.01.008
34. Pan H, Zhao X, Darvell BW, Lu WW (2010) Acta Biomater 6:4181. doi:10.1016/j.actbio.2010.05.013
35. Gibson IR, Best SM, Bonfield W (2002) J Am Ceram Soc 85:2771. doi:10.1111/j.1151-2916.2002.tb00527.x
36. Kim SR, Lee JH, Kim YT, Riu DH, Jung SJ, Lee YJ, Chung SC, Kim YH (2003) Biomaterials 24:1389. doi:10.1016/s0142-9612(02)00523-9
37. Qiu ZY, Li G, Zhang YQ, Liu J, Hu W, Ma J, Zhang SM (2012) Biomed Mater 7:045009. doi:10.1088/1748-6041/7/4/045009
38. Tian T, Jiang D, Zhang J, Lin Q (2008) Mater Sci Eng C 28:57. doi:10.1016/j.msec.2007.10.049
39. Aminian A, Solati-Hashjin M, Samadikuchaksaraei A, Bakhshi F, Gorjipour F, Farzadi A, Moztarzadeh F, Schmuecker M (2011) Ceram Int 37(4):1219. doi:10.1016/j.ceramint.2010.11.044
40. Arcos D, Rodriguez-Carvajal J, Vallet-Regí M (2004) Chem Mater 16:2300. doi:10.1021/cm035337
41. Gibson IR, Hing KA, Revell PA, Santos JD, Best SM, Bonfield W (2002) Key Eng Mater 218-220:203. doi:10.4028/www.scientific.net/KEM.218-220.203
42. Leventouri T, Bunaciu CE, Perdikatsis V (2003) Biomaterials 24:4205. doi:10.1016/s0142-9612(03)00333-8
43. Palard M, Champion E, Foucaud S (2008) J Solid State Chem 181:1950. doi:10.1016/j.jssc.2008.04.027
44. Arcos D, Rodriguez-Carvajal J, Vallet-Regí M (2004) Solid State Sci 6:987. doi:10.1016/j.solidstatesciences.2004.05.001
45. Aguiar H, Serra J, Gonzalez P, Leon B (2009) J Non-Cryst Solids 355:475. doi:10.1016/j.jnoncrysol.2009.01.010
46. Bianco A, Cacciotti I, Lombardi M, Montanaro L (2009) Mater Res Bull 44:345. doi:10.1016/j.materresbull.2008.05.013
47. Sudarsanan K, Young RA (1969) Acta Crystallogr B 25:1534. doi:10.1107/s0567740869004298
48. Hartmann P, Jäger C, Barth S, Vogel J, Meyer K (2001) J Solid State Chem 160:460. doi:10.1006/jssc.2001.9274
49. Yu H, Zhang H, Wang X, Gu Z, Li X, Deng F (2007) J Phys Chem Solids 68:1863. doi:10.1016/j.jpcs.2007.05.020
50. Isobe T, Nakamura S, Nemoto R, Senna M, Sfihi H (2002) J Phys Chem B 106:5169. doi:10.1021/jp0138936
51. Wilson RM, Elliott JC, Dowker SEP, Rodriguez-Lorenzo LM (2005) Biomaterials 26:1317. doi:10.1016/j.biomaterials.2004.04.038
52. Gomes S, Renaudin G, Mesbah A, Jallot E, Bonhomme C, Babonneau F, Nedelec JM (2010) Acta Biomater 6:3264. doi:10.1016/j.actbio.2010.02.034
53. Li XW, Yasuda HY, Umakoshi Y (2006) J Mater Sci Mater Med 17:573. doi:10.1007/s10856-006-8942-2
54. Thian ES, Huang J, Best SM, Barber ZH, Bonfield W (2006) J Biomed Mater Res 76B:326. doi:10.1002/jbm.b.30368
55. Porter AE (2006) Micron 37:681. doi:10.1016/j.micron.2006.03.006
56. Vandiver J, Dean D, Patel N, Botelho C, Best S, Santos JD, Lopes MA, Bonfield W, Ortiz C (2006) J Biomed Mater Res 78A:352. doi:10.1002/jbm.a.30737